Thermopower and resistivity of the topological insulator Bi_2Te_3 in the amorphous and crystalline phase

OPEN ACCESS
IOP Publishing
Journal of Physics: Condensed Matter
J. Phys.: Condens. Matter **36** (2024) 355001 (9pp)
https://doi.org/10.1088/1361-648X/ad5095

Thermopower and resistivity of the topological insulator Bi_2Te_3 in the amorphous and crystalline phase

E Osmic[1,2,*], J Barzola-Quiquia[3,4], S Winnerl[5], W Böhlmann[6] and P Häussler[3]

[1] Dresden High Magnetic Field Laboratory (HLD-EMFL), Helmholtz-Zentrum Dresden-Rossendorf, Dresden 01328, Germany
[2] Institut für Festkörper- und Materialphysik, Technische Universität Dresden, Dresden 01062, Germany
[3] Division of Thin Films Physics, Institute of Physics, Chemnitz University of Technology, Chemnitz 09107, Germany
[4] Advanced Technologies Division/R&D, FHR Anlagenbau GmbH, Am Hügel 2 Ottendorf-Okrilla, 01458, Germany
[5] Institute of Ion Beam Physics and Materials Research, Helmholtz-Zentrum Dresden-Rossendorf, Dresden 01328, Germany
[6] Felix-Bloch Institute for Solid-state Physics, University of Leipzig, Linnéstrasse 5, Leipzig 04103, Germany

E-mail: e.osmic@hzdr.de

Received 26 February 2024, revised 13 May 2024
Accepted for publication 24 May 2024
Published 7 June 2024

Abstract

We have, *in-situ*, prepared and measured the temperature dependence of thermopower $S(T)$ and resistance $R(T)$ of Bi_2Te_3 topological insulator (TI) thin films in the amorphous and crystalline phase. Samples were prepared by sequential flash-evaporation at liquid ^{4}He temperature. The $S(T)$ in the amorphous phase is negative and much larger compared to other known amorphous materials, while in the crystalline phase it is also negative and behaves linearly with the temperature. The resistivity $\rho(T)$ in the amorphous phase shows a semiconducting like behavior that changes to a linear metallic behavior after crystallization. $S(T)$ an $\rho(T)$ results in the crystalline phase are in good agreement with results obtained both in bulk and thin films reported in the literature. Linear behavior of the $\rho(T)$ for $T > 15$ K indicates the typical metallic contribution from the surface states as observed in other TI novel materials. The low temperature conductivity $T < 10$ K exhibits logarithmic temperature dependent positive slope $\kappa \approx 0.21$, indicating the dominance of electron-electron interaction (EEI) over the quantum interference effect, with a clear two dimensional nature of the contribution. Raman spectroscopy showed that the sample has crystallized in the trigonal $R\bar{3}m$ space group. Energy-dispersive x-ray spectroscopy reveales high homogeneity in the concentration and no magnetic impurities introduced during preparation or growth.

Keywords: thermopower, power factor, electron-electron interaction, Raman spectroscopy, amorphous and crystalline topological insulator Bi_2 Te_3

* Author to whom any correspondence should be addressed.

1. Introduction

Topological insulators (TI) are a new class of materials, which were theoretically predicted to exist in different Bi, Sb and Te based compounds [1–3]. Angle-resolved photoemission spectroscopy (ARPES) has been used to verify the topological surface states of such materials [4–6]. TI have, due to strong spin–orbit coupling, an insulating bulk energy gap and generate conducting topologically protected gapless electronic surface states, which are robust against disorder and magnetic impurities [7]. These new materials have very interesting properties from the basic physics point of view and for future applications, for example, the observation of the quantum spin Hall effect or the realization of Majorana fermions for the application in topological quantum computation [8, 9]. The alloy Bi_2Te_3 was proposed as a three-dimensional (3D) TI, and later it was experimentally confirmed by ARPES [6] that this system possesses a single Dirac cone on the surface. Transport properties of different TIs, including Bi_2Te_3, were extensively studied and it had been observed that these materials exhibit a wide variety of exotic electric transport properties like extremely large *MR*, high carrier mobility μ, light effective mass, nontrivial Berry phase, and the anomalous Hall effect [10].

Since the 1950s [11], it is well known that those materials, today called TIs, are the best thermoelectrics (TE) at room temperature, with the most special being Bi_2Te_3 in its bulk form and known as one of the best TE materials for application at room temperature and above (270–400 K) with the dimensionless high figure of merit $Z = S^2\sigma/(\kappa_e + \kappa_{ph}) \approx 1$ [12], where σ is the electric conductivity, $\kappa = \kappa_e + \kappa_{ph}$ is the thermal conductivity, consisting of a contribution from electrons κ_e and phonons κ_{ph}, and S is the thermopower. So, in order to improve the performance of TE it is necessary to increase the power factor defined as $PF = S^2\sigma$, which is mainly associated to the electronic part of materials [13].

The influence of TI boundary states has long been neglected in early thermoelectric research due to the lack of information of its existence. In recent years this neglected issue has attracted intensive research efforts from the theoretical and experimental point of view to explore the contribution of TI boundary states to thermoelectricity. For example, Dirac fermions in topological edge and surface states are robust against backscattering with defects in the crystal structure and magnetic and non magnetic impurities [14]. This opens the possibility of creating an ideal thermoelectric material that combines the properties of a *phonon-glass electron-crystal* proposed by Slack [15]. Summarizing the idea, creating a large number of defects in a TI, e.g. using ion irradiation, it is possible to considerably reduce its lattice thermal conductivity κ_{ph} while retaining the high electrical conductivity of topological surface states. First theoretical predictions of topological phases of matter are said to be ubiquitous in crystals, but less is known about their existence in amorphous systems that lack long-range order but possess well-defined local order that involves, up to, neighbors larger than the fifth order [16, 17]. But in recent years new theoretical studies have appeared stating that there is the possibility of realizing topological phases in amorphous systems [18, 19]. Very recently, the observation of topological states in a sample of amorphous Bi_2Se_3 has been experimentally demonstrated. The authors have shown that applying a magnetic field to amorphous Bi_2Se_3, a typical weak anti-localization was observed in the magnetoresistance at small magnetic fields. Additionally, ARPES supports the topological state interpretation with data showing consistency with a dispersive two-dimensional surface state that crosses the bulk gap [20].

In the present research, for the first time in the literature, we are presenting a detailed study of the thermopower $S(T)$ and the resistivity $\rho(T)$ of a Bi_2Te_3 thin film in the amorphous and crystalline phase, this was possible only because of the preparation method and the low temperature cryostat used. All results from the amorphous phase are unique and new, while the crystalline phase results are very similar to those from the literature, where samples were prepared with more expensive and sophisticated methods. The results of the crystallized sample evidently show contribution in the $S(T)$ and $\rho(T)$ of the 2D topological protected surface, while we cannot state that the results of the amorphous phase have a topological character, due to the limitations of magnetic fields during the measurements and the lack of theory that supports the results of thermopower.

2. Experimental details

Bi_2Te_3 alloys were prepared by melting pure bismuth and tellurium (purity 99.9999%, Alfa Aesar) in proper atomic proportions in an evacuated quartz ampoule at a base pressure of approximately $P \approx 10^{-7}$ mbar. After the alloy was removed from the ampoule and milled into pieces of 200–300 μm in diameter, it was introduced into a chamber for *in-situ* film preparation and measurement. The amorphous Bi_2Te_3 thin film was prepared by rapid quenching at liquid ^{4}He temperature under high vacuum conditions ($\approx 5 \times 10^{-7}$ mbar), i.e. the technique called flash evaporation, which was already used successfully to prepare TI films of Bi_2Se_3 [21] and $Bi_{100-x}Sb_x$ [22]. The absolute Seebek coefficient $S(T)$ was measured between 5 and 325 K by applying a slowly alternating temperature gradient across the thin film as described in the literature [22–24]. The temperature dependence of resistance $R(T)$ was measured parallel to the $S(T)$ between 1.2 and 345 K, for that the film was structured in an conventional 4-point shape. After the sample was characterized in $S(T)$ and $R(T)$, it was removed from the cryostat for additional *ex-situ* sample characterization at room temperature. At this point we want to comment that due to the *in-situ* experimental conditions used in this work, where simultaneous measurements of resistance and thermopower are being performed, the setup does not allow for additional spectroscopic measurements (such as XPS, Raman, XRD, LEED etc). For this reason we have only structurally characterized the crystallized sample. Elemental analysis to determine the atomic composition was performed using the energy-dispersive x-ray (EDX) spectrometer coupled with a FEI NanoLab XT 200 Dual-Beam microscope, film thickness was determined by AFM and finally Raman spectroscopy

measurements were performed with a LabRAM HR Evolution spectrometer, using wavelength of $\lambda = 532$ nm.

3. Results and discussion

3.1. Temperature dependence of the resistivity and thermopower

3.1.1. Resistivity in the amorphous and crystalline phase. Temperature dependence of the resistivity $\rho(T)$ in the amorphous and crystalline phase of the investigated Bi_2Te_3 thin film are shown in figure 1(a). The $\rho(T)$ in the amorphous phase was measured immediately after preparation, i.e. the data were obtained during annealing and are non irreversible results (indicated with $\longrightarrow$ in figure 1(a), and after maximal annealing temperature was reached, the sample was again cooled and the $\rho(T)$ measured by increasing the temperature. These results are reversible and are indicated with double arrow ($\longleftrightarrow$) in figure 1(a). After preparation, the amorphous Bi_2Te_3 has a large resistivity which decreases by increasing the temperature in a non activated temperature behavior, and approximately at $T_K \approx 269$ K the film crystallizes, this is evident by the rapid and huge decrease of the resistivity, a common method to identify crystallization temperature of amorphous materials [25–28]. After crystallization, the ρ behaves linearly during annealing up to $T = 345$ K. We observe a remarkable behavior of the amorphous $\rho(T)$ at low temperatures, as can be seen in the inset of figure 1(a), a drop in the $\rho(T)$ is observed starting at $T = 2.29$ K and reaching $\rho(T) = 0$ at $T_0 = 0.78$ K (determined by linear extrapolation). This behavior we interpret as a sign of superconductivity, which was already observed in amorphous TI samples of $Bi_{100-x}Sb_x$ [24]. The fact that we cannot measure zero resistance is because we could not cool down our sample lower than 1.2 K. Another argument supporting our statement is based on the observation of phonon-induced electron-electron interaction in disordered superconductors [29]. It was established experimentally, as well theoretically, that the effects of electron–electron (e–e) interaction in 3D disordered superconductors cause a resistivity change at low temperatures (i.e. in the residual resistivity regime) given by [30]

$$\frac{\Delta\rho(T)}{\rho} = -\frac{0.919e^2}{4\pi^2\hbar}\left[\frac{4}{3} - \frac{3}{2}\tilde{F} - \frac{2}{\ln(T_c/T)}\right] \times \rho\left[\frac{k_B T}{\hbar D}\right]^{1/2}, \quad (1)$$

where e is the electronic charge, k_B is the Boltzmann constant, $\hbar$ is the Planck constant divided by 2π, D is the diffusion constant, $\tilde{F}$ is the electron screening parameter and T_c the superconducting transition temperature [30]. In order to use the equation (1) to fit our results, it is necessary to have the value of D, which was obtained in similar experiments by measuring the magnetoresistance [31, 32], which was not possible in our case. For this reason, in order to have a qualitative description of our results, we have rewritten the equation as following, $\Delta\rho(T)/\rho_0^2 = -P_1 T^{1/2} + P_2 T^{1/2}/\ln(T_c/T)$ and added the contribution of the usual Boltzmann transport term $P_3 T^5 + P_4$, similar as done in the literature [29, 31, 33], with the constants

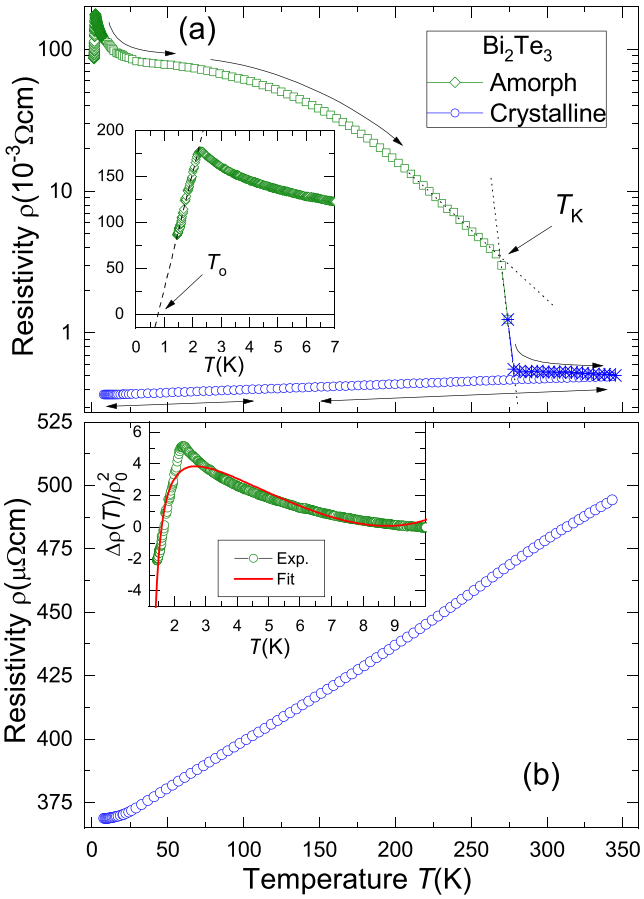

Figure 1. Temperature dependence of the resistivity $\rho(T)$. In (a) results of the amorphous and crystalline phase. In (b) results of the crystalline phase. The inset in (a) shows the lowest temperature of the resistivity in the amorphous phase. The inset in (b) shows the fit using the modified equation (1).

P_i with $i = 1, 2, 3, 4$ and T_c being the fit parameters. The experimental $\Delta\rho(T)/\rho_0^2$, with $\rho_0 = \rho(T = 10\,\text{K})$, and the fit result are shown in the inset of figure 1(b). It can be seen that the fit describes the experimental data well, with the parameters $P_1 = 5.16 \times 10^{-6}, P_2 = 3.6 \times 10^{-6}, P_3 = 2.99 \times 10^{-11}, P_4 = 1.9 \times 10^{-5}$ and $T_c = 1.02$ K, a value little higher that the one predicted when we extrapolate the experimental results to zero resistance. This result leads us to state that it is highly probable that the Bi_2Te_3 in the amorphous phase is superconductor, similar as the TI $Bi_{100-x}Sb_x$ in the amorphous phase. It should be noted that by doping Bi_2Te_3 with Pd Hor *et al*, have reported superconductivity with a $T_c = 5.5$ K [34].

In the crystalline phase, in general, $\rho(T)$ of the Bi_2Te_3 film shows a linear metallic behavior as shown in figure 1(b), very similar as in the case of other TI Bi_2Te_3 thin films prepared with different techniques, such as molecular beam epitaxy [35, 36], metal organic chemical vapor deposition [37] and DC magnetron sputtering [38]. The estimated resistivity of our Bi_2Te_3 thin film is in the same order as in thin films [38, 39] and bulk [34] samples of Bi_2Te_3 reported in the literature. We have payed attention to the low temperature results (i.e. $T < 10$ K) and plotted in figure 2 the results of the resistivity

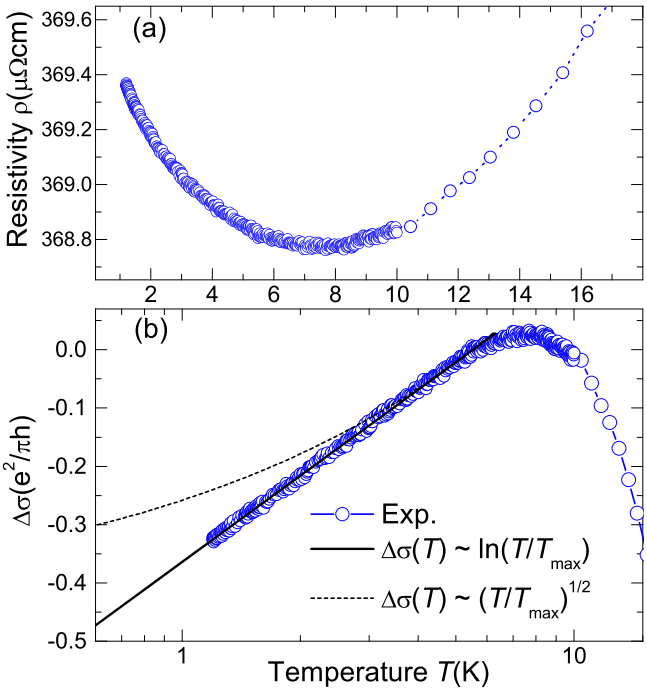

Figure 2. Low temperature results of the crystalline phase, in (a) the resistivity $\rho(T)$ and in (b) the corresponding conductivity normalized in units of $e^2/\pi h$.

vs temperature and the conductivity (in units of $e^2/\pi h$) vs the temperature in logarithmic scale. It is evident that for $T \lessapprox 8$ K the $\rho(T)$ exhibits an upturn by decreasing the temperature. This behavior was already reported in films [40] and bulk [41] samples of the TI Bi_2Te_3 and Bi_2Se_3 [42].

According to many literature results, both theory [43] and experiments, it was established that in many TI materials (non magnetic doped) quantum interference effect (QIE), i.e. weak localization, weak antilocalization, and many-body disorder-enhanced electron-electron Coulomb interaction (EEI) dominate the conductivity at low temperature and are responsible for the upturn in the resistivity.

Assuming that both QIE and EEI contribute to the conductivity at low temperatures ($T < 8$ K in our case), the total correction $\Delta\sigma(T)$ of conductivity can be expressed as:

$$\Delta\sigma\,(T) = \sigma_0 + \Delta\sigma\,(T)^{\mathrm{EEI}} + \Delta\sigma\,(T)^{\mathrm{QIE}}, \tag{2}$$

with

$$\Delta\sigma\,(T)^{\mathrm{EEI}} = \sigma_0 + \frac{e^2}{\pi h}\left[1 - \frac{3F}{4}\right]\ln\left(\frac{T}{T_{\mathrm{EEI}}}\right), \tag{3}$$

and

$$\Delta\sigma\,(T)^{\mathrm{QIE}} = p\alpha\frac{e^2}{\pi h}\ln\left(\frac{T}{T_{\mathrm{QIE}}}\right) \tag{4}$$

where σ_0 is the Drude conductivity ($ne^2\tau/m_e$), n is the electron density, m is the mass of electron, τ is the relaxation time, F is the dimensionless screened Coulomb potential between electrons averaged over the Fermi surface [30], and T_{EEI} is the characteristic temperature below which logarithmic-dependent conductivity due of EEI starts to dominate.

The dimensionless parameter p depends on various sources of inelastic scattering that destroy phase coherence and in a 2D disordered electronic system $p = 1$ for EEI, α is a dimensionless coefficient in Hikami-Larkin-Nagaoka (HLN) theory and T_{QIE} is the characteristic temperature, above which the conductivity corrections due to QIE vanish.

Following literature works [40, 44–46], in order to analyze our results, in our case we may assume without any loss of generality, that $T_{\mathrm{EEI}} = T_{\mathrm{QIE}} = T_{\max} = 5.5$ K, where the conductivity of the material reaches its maximum as the characteristic temperature below which these corrections is valid. So, finally the equation (2) in the unit of $e^2/\pi h$ can be written as following:

$$\Delta\sigma\,(T) = \sigma_0 + \kappa\ln\left(\frac{T}{T_{\max}}\right) \tag{5}$$

where $\Delta\sigma(T) = [\sigma(T) - \sigma(T = T_{\max})]$, κ is the slope of $\Delta\sigma(T)$ vs $\ln(T)$ curve and it can be expressed as $\kappa = (1 + \alpha p - 3F/4) = \frac{\partial\Delta\sigma}{\partial\ln(T)}$, with F the Coulomb screening factor that quantifies the screened Coulomb interaction [29, 47]. The obtained value of κ from the fits to $\Delta\sigma(T)$ shown in figure 2(b) is $\kappa = 0.212\,83 \pm 0.000\,46$. It was determined that in TI materials, κ is always positive due to the dominance of the EEI effect [43, 44] over the QIE. In figure 2(b) we have also plotted (as dashed lines) a correction of electrical conductivity $\Delta\sigma(T)$ because of the EEI in 3D materials at low temperatures, i.e. $\Delta\sigma(T) \propto \sqrt{T}$, evidencing that rightly so we can discard at all the 3D nature of the correction.

Considering the values obtained in the literature for bulk and thin films of Bi_2Te_3, we assume $p = 1$ and $\alpha = -1/2$, values obtained after fitting the conductance $\Delta\sigma(B) = \sigma(B) - \sigma(0)$ as a function of the perpendicular magnetic field within the framework of the HLN theory [40, 48–50]. Thus, using the above mentioned values for p and α, we obtain $F = 0.382$. According to the theory within the Thomas–Fermi approximation it is predicted $-1 \leqslant F \leqslant 1$, $F \to 0$ in the limit of no screening (or, bad conductors), while $F \to 1$ in the limit of complete screening (or, good metals) [30, 47]. The obtained value is very similar to the one reported for thin films of Bi_2Te_3 [40, 51] and Bi_2Se_3 [42], not only in absolute value but also in sign. Another scattering mechanism which produce an logarithmic upturn in the resistivity at low temperatures is the Kondo effect [52, 53], due to magnetic impurities, probably introduced during the sample preparation. This contribution we discard, because its very well known that thermopower is very sensitive to magnetic impurities scattering, manifesting as a bump-shaped feature at low temperatures as shown in figure 3(b). This figure serves as an example of what was measured in Au containing ≈10 ppm of Fe.

3.1.2. Themopower in the amorphous and crystalline phase. Thermopower results in the amorphous ad crystalline phase are plotted in figure 3. The $S(T)$ in the amorphous phase is negative and increases its magnitude by increasing the temperature up to 200 K to later slowly change its slope and when the sample

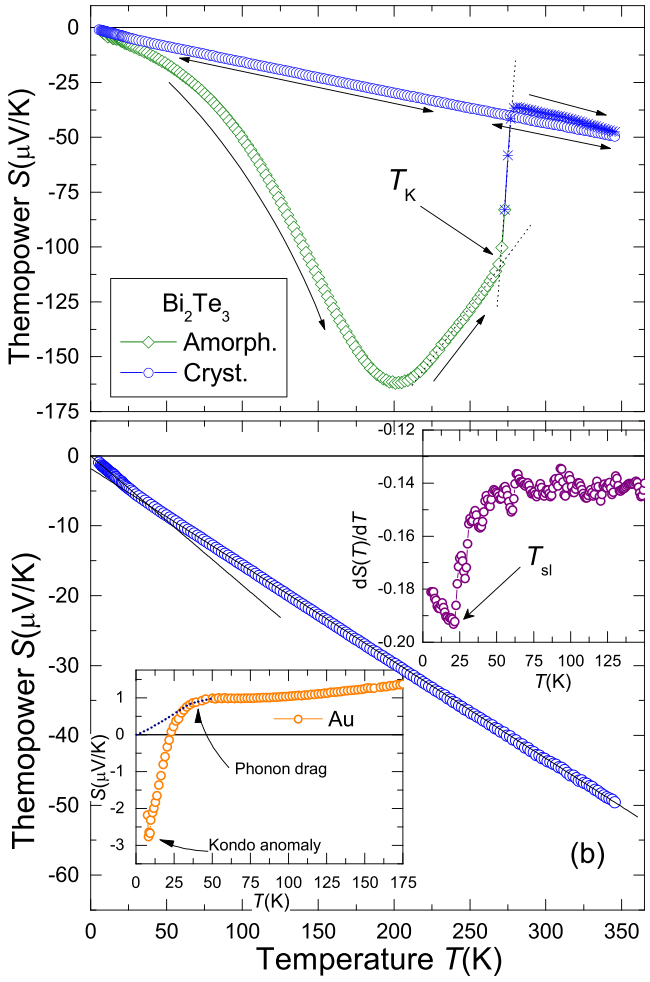

Figure 3. Temperature dependence of the thermopower $S(T)$. In (a) results of the amorphous phase, during crystallization and crystalline phase. In (b) results of the crystalline phase. The down inset in (b) are results from a crystalline Au sample and upper one is the derivative of the thermopower of our crystallized sample.

starts to crystallize, a sharp change in the $S(T)$ is observed. The temperature at which the sample crystallizes visible by the $S(T)$ results is the same as observed by the resistance measurements. Above T_K the $S(T)$ still shows a negative slope and increases in magnitude by increasing the temperature. The absolute value of the $S(T)$ of the amorphous Bi_2Te_3 is large in comparison to other amorphous metallic alloys, e.g. they reach a value of $S(T = 200\,\mathrm{K}) < 2\mu\,\mathrm{V\,K^{-1}}$ [54], i.e. two orders less than in our investigated sample. After maximal annealing at $T = 345$ K the crystallized sample was cooled and again the $S(T)$ measured, in order to make that more evident, we have plotted the results in the figure 3(b) which show negative thermopower over the entire range of temperatures. The negative $S(T)$ in Bi_2Te_3 samples is because its Fermi energy E_F lies in the bulk conduction band due the n-type bulk carriers induced by Te vacancies, as confirmed by the Hall effect [36] and ARPES measurements [35]. As it can be seen, the thermopower of the crystallized sample behaves almost linearly in all temperatures measured, but careful observation leads us to see that there is a fast change in the slope at $T_{sl} \approx 25$ K which is made clear by linear fits shown in the figure 3(b) and more evident if we plot the first derivative $\mathrm{d}S(T)/\mathrm{d}T$, as shown as inset in the same figure. From our knowledge, there is no theory discussing such behavior, although observed in some experimental works [36, 40], pointing out the mentioned regions with linear behavior but not discussed [40] explicitly. But we do have an idea of where this is coming from. If we take into account diverse results in the literature, where magnetotransport properties are investigated, we can observe that one parameter which changes steadily with the temperature is the phase coherence length l_ϕ, which signifies the length over which an electron can move without losing the phase of its eigenstate [55]. Literature results of Bi_2Te_3 [48, 51] show that the $l_\phi(T)$ tends to have a value close to zero at approximately $T \approx 25$ K, which is similar to the temperature T_{sl}. To remark, the steady decrease in l_ϕ with temperature is expected because of the increased elastic and inelastic scattering of charge carriers by impurities and phonons [56], and we believe that it is the reason for the slope change in $S(T)$, at the same range of temperature. The change of slope can not be related to some magnetic impurities as the effect of only a few ppm is already noticeable. An example is thermopower of gold containing ≈10 ppm of Fe plotted as inset in figure 3(b), the deep negative peak in $S(T)$ is a consequence of the Kondo effect [57], which in this specific case even originated a change in the sign of $S(T)$. The dotted lines indicate what we would observe without Fe impurities and the peak around 35 K is identified as consequence of the phonon drag effect [57].

3.2. Power factor in the amorphous and crystalline phase

The temperature-dependent power factors $PF(T)$ in the amorphous and crystalline phase for the studied Bi_2Te_3 sample have been obtained from $\rho(T)$ and $S(T)$ results and are shown in figure 4. Generally, in both phases, the $PF(T)$ increases with T, without displaying any maximum up to the maximum temperature used in this investigation. The PF in the amorphous phase is almost negligible for temperature $T < 100$ K for later increase up to the temperature where the sample crystallizes. During the crystallization the PF decreases suddenly for after increase by increasing the temperature (shown as star symbols in figure 4). When we compare the PF of both phases we can observe that for temperature $230\,\mathrm{K} < T < 270\,\mathrm{K}$, the PF corresponding to the amorphous phase is evidently larger than that from the crystalline phase. If we take into the consideration that the thermal conductivity κ of the amorphous phase is less than in the crystalline phase, mainly due to phonon contribution κ_{ph}, we can state that the figure of merit Z of the amorphous phase is larger than in the crystalline phase, probably in a larger range of temperature than the one mentioned above. From the PF results in the crystalline phase we can observe that it behaves almost quadratic with the temperature, as shown by the fit done and plotted as line in the same figure. Using the extrapolated data we have compared our PF with those from the literature for higher temperatures as shown in the inset of figure 4, showing that our results are in good agreement with the literature where samples were prepared

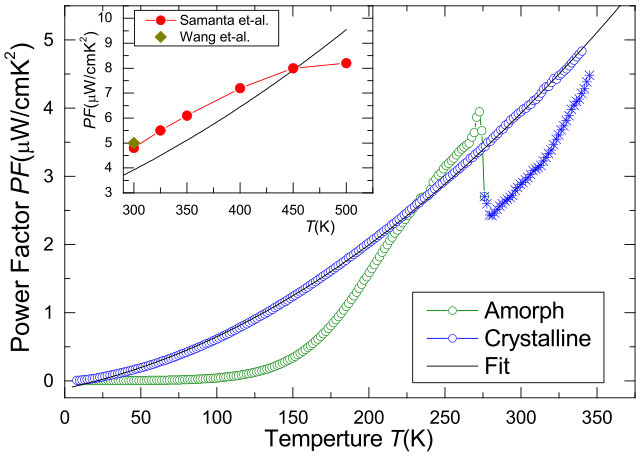

Figure 4. Temperature dependence of the power factor $PF(T)$ of the amorphous and crystallized phase of Bi_2Te_3 thin film. The symbols are results during and after crystallization as explained in the text. The inset is our extrapolated data compared with results from the literature.

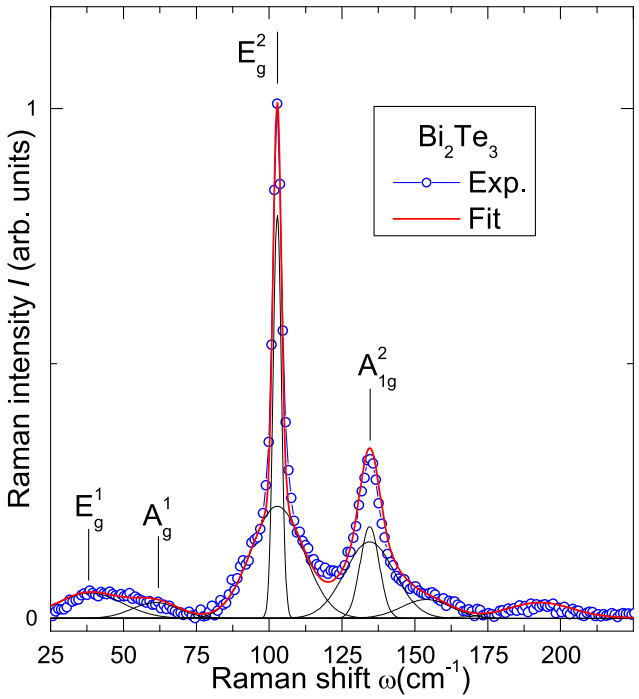

Figure 5. Raman spectra of the crystallized phase of Bi_2Te_3 thin film.

with more complex methods and annealed to 650 K [58] and 423 K [59], respectively.

3.3. Raman spectroscopy

Raman spectroscopy is used in the last years as powerful method to provide useful structural information, crystalline phase, composition, and stoichiometry of different TI samples [60, 61]. We have performed Raman measurements on our sample at ambient conditions after the sample was annealed at $T = 345$ K and the results are shown in figure 5. After analyzing the Raman results (figure 5) by Gaussian fitting, the frequencies of the peaks and their assignment are listed in the table 1, together with the previously reported data from the literature in bulk and similar film thickness. In figure 5 we can see that to obtain a good fit of the most relevant peaks of the Raman spectrum, we have used two Gaussians in the same position but with different intensities and widths. We interpret this as necessary since our sample is polycrystalline and there must be regions of the sample with crystalline structure of nanometric size (or perhaps also grain boundaries). This interpretation is supported by the Raman results of the TI Sb_2Te_3 [62], where the Raman spectral evolution through amorphous to crystalline transitions was studied, and shown that Raman peaks immediately after crystallization are wide and not very intense. The use of Gaussian peaks that are not indexed can be attributed to surface oxidation, also observed in other thin films [63, 64] but not in the case of *in-situ* Raman measurements of a ≈40 nm thick sample [65].

Considering the experimental resolution, one can see that the peak positions of the most characteristic expected optical phonon modes are in good agreement with the previously reported data of Bi_2Te_3 in the literature [61, 64–66]. The Raman results shown in figure 5 and the corresponding assignment, indicate that our preparation method (after annealing) leads to obtain well ordered crystalline films of Bi_2Te_3, with the corresponding crystal structure belonging to the space group $R\bar{3}m(D^5_{3d})$ [67].

3.4. EDX spectroscopy

These experiments were done at room temperature after the transport measurements were performed. It is here important to note that up to this point the samples were exposed to air for more than six months. The main aim of this experiment was to confirm the nominal composition and if it was maintained in comparison to the starting one, as well as to determine if some ferromagnetic contaminants were present in the sample. One example of the result is shown in figure 6, where peaks corresponding to Bi and Te are evidently observable, as well as the presence of peaks related to the oxygen. As we mentioned, before EDX measurements, the sample was exposed to air and its well known that a oxidation process occurs. The oxidation was confirmed by XPS measurements in the literature [68, 69]. So, without losing generality, we have quantified the results without considering the oxygen contribution and calculated the sample composition from the EDX results obtained at three different parts of the sample. The results are presented in the table 2. Besides confirming the absence of ferromagnetic impurities within the detection limits of this technique, EDX analysis allowed to verify that the actual composition of the samples agrees with the nominal value with an error of of $\pm 1.3\%$, confirming that our synthesis method (sequential flash evaporation) is very accurate in producing the desired composition and in a good agreement with previous results of other TIs prepared by the same technique like $Bi_{60}Se_{40}$ [21] and $Bi_{100-x}Sb_x$ [22, 24]. We emphasize the EDX results regarding

Table 1. Identified Raman peaks and widths (FWHM) in units of cm^{-1}. The first row are data of this work while the other rows are from the literature. The samples thickness is *d*.

d (nm)	E_g^1	A_{1g}^1	E_g^2/FWHM	A_{1g}^2/FWHM
63	38	62	102.8/4.2	134.6/11
50 [61]	39	61.1	101.5	132.4
82 [66]	38.5	61.5	101.9	132.7
830 [64]	—	60.9	101.2/3.7	133.0/9
Bulk [66]	34.4	62.1	101.7	134.0
Bulk [67]	36.5	62.0	102.3/6	134.0/10

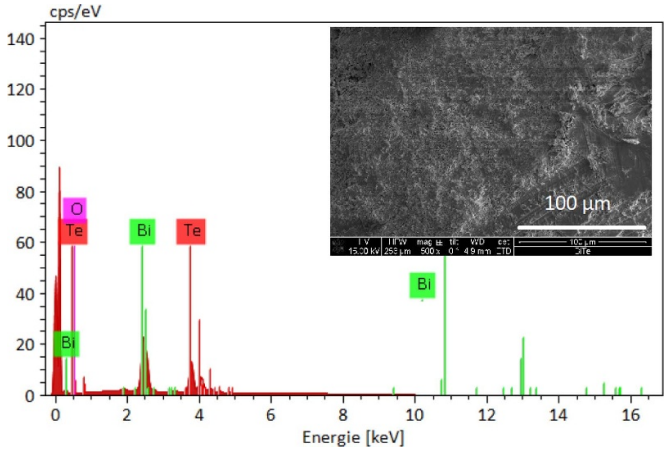

Figure 6. EDX spectrum obtained for sample $Bi_{40}Te_{60}$ at the position P_{o1}. The inset shows a scanning electron microscope (SEM) image of the investigated sample at position P_{o1}.

Table 2. Elemental composition of the $Bi_{40}Te_{60}$ sample obtained at two (P_{o1}, P_{o2}) different positions in the sample.

Element	P_{o1} (Atom%)	P_{o2} (Atom%)	Abs. Error
Bi	40.17	40.84	±0.01%
Te	59.84	59.16	±0.01%

the ferromagnetic impurities such as Fe, Co and Ni, because this supports the interpretation that the upturn of the $R(T)$ at low temperatures is due to the EEI interaction and not because of some ferromagnetic centers scattering process.

4. Conclusions

We have prepared Bi_2Te_3 thin films samples by the sequential flash evaporation method in the amorphous and crystalline phase and measured *in-situ* the thermopower and resistance. The amorphous film shows a huge and semiconductor-like type resistivity, with a peculiar rapid decreasing for temperatures $T < 2.3$ K which we interpret as a sign of a probable superconducting transition as observed in amorphous TI $Bi_{100-x}Sb_x$, while the thermopower also shows huge negative values up to when crystallization occurs. In the crystalline phase, the $\rho(T)$ is metallic in all ranges of temperature measured, except for $T < 10$ K, where we have described the upturn in $R(T)$ because of the EEI. Thermopower in the crystalline phase shows linear behavior in two regions, one down to $T \approx 25$ K and above another, our $S(T)$ results are in agreement with literature results, where linearity was observed in similar samples and other TI alloys. Raman results are in good agreement with the expected peaks for a well ordered Bi_2Te_3, corresponding to the crystal structure belonging to the space group $R\bar{3}m(D_{3d}^5)$, and finally EDX results confirm that our preparation method retained the initial concentration and that during the film production process no magnetic impurities were introduced. We want to conclude by mentioning that our preparation method not only leads us to obtain high quality films, but there will also be the opportunity to prepare thin films in the amorphous phase to stepwise investigate the changes in their electronic (as well as magnetic) properties in its evolution towards crystalline transformation. In addition, our preparation method is compatible with processes that include lithography, giving the opportunity to study bilayers between TIs or with other non-magnetic and magnetic materials, and exploration of new properties for future applications.

Data availability statement

All data that support the findings of this study are included within the article (and any supplementary files).

Acknowledgments

We are thankful to Dr C Lauinger for the Au thermopower measurements. We would like to thank Mrs. Lucchesi, for the support during Raman measurement.

ORCID iDs

E Osmic https://orcid.org/0000-0003-2513-0074
J Barzola-Quiquia https://orcid.org/0000-0003-1716-4493

References

[1] Fu L, Kane C L and Mele E J 2007 Topological insulators in three dimensions *Phys. Rev. Lett.* **98** 106803
[2] Teo J C Y, Fu L and Kane C L 2008 Surface states and topological invariants in three-dimensional topological insulators: application to $Bi_{1-x}Sb_x$ *Phys. Rev.* B **78** 045426
[3] Zhang H, Liu C, Qi X, Dai X, Fang Z and Zhang S 2009 Topological insulators in Bi_2Se_3, Bi_2Te_3 and Sb_2Te_3 with a single Dirac cone on the surface *Nat. Phys.* **5** 438
[4] Hsieh D *et al* 2009 Observation of unconventional quantum spin textures in topological insulators *Science* **323** 919

[5] Xia Y *et al* 2009 Observation of a large-gap topological-insulator class with a single Dirac cone on the surface *Nat. Phys.* **5** 398

[6] Chen Y L *et al* 2009 Experimental realization of a three-dimensional topological insulator, Bi_2Te_3 *Science* **325** 178

[7] Hasan M Z and Kane C L 2010 Colloquium: topological insulators *Rev. Mod. Phys.* **82** 3045

[8] Qi X-L and Zhang S-C 2010 The quantum spin Hall effect and topological insulators *Phys. Today* **63** 33

[9] Beenakker C W J 2013 Search for Majorana fermions in superconductors *Annu. Rev. Condens. Matter Phys.* **4** 113

[10] Hu J, Xu S-Y, Ni N and Mao Z 2019 Transport of topological semimetals *Annu. Rev. Mater. Res.* **49** 207–52

[11] Goldsmid H J and Douglas R W 1954 The use of semiconductors in thermoelectric refrigeration *Br. J. Appl. Phys.* **5** 386

[12] Tritt T M 2015 Holey and unholey semiconductors *Science* **283** 804

[13] Bergman D J and Fel L G 1999 Enhancement of thermoelectric power factor in composite thermoelectrics *J. Appl. Phys.* **85** 8205

[14] Liu M *et al* 2012 Crossover between weak antilocalization and weak localization in a magnetically doped topological insulator *Phys. Rev. Lett.* **108** 036805

[15] Slack G A 1995 *CRC Handbook of Thermoelectrics* (CRC Press)

[16] Barzola-Quiquia J and Häussler P 2002 On the structure of semiconducting amorphous systems 2002 *J. Non-Cryst. Solids* **299–302** 269

[17] Barzola-Quiquia J, Osmic E and Häussler P 2021 The magnetic properties of amorphous Al_xFe_{100-x} alloys investigated by the atomic structure, magnetoresistance and anomalous Hall effect *J. Magn. Magn. Mater.* **526** 167624

[18] Agarwala A and Shenoy V B 2017 Topological insulators in amorphous systems *Phys. Rev. Lett.* **118** 236402

[19] Mitchell N P, Nash L M, Hexner D, Turner A M and Irvine W T M 2018 Amorphous topological insulators constructed from random point sets *Nat. Phys.* **14** 380

[20] Corbae P *et al* 2023 Observation of spin-momentum locked surface states in amorphous Bi_2Se_3 *Nat. Mater.* **22** 200

[21] Barzola-Quiquia J, Lehmann T, Stiller M, Spemann D, Esquinazi P and Häussler P 2015 Topological insulator thin films starting from the amorphous phase-Bi_2Se_3 as example *J. Appl. Phys.* **117** 075301

[22] Osmic E, Barzola-Quiquia J, Böhlmann W, Bercoff P G, Venosta L and Häussler P 2022 Thermopower and magnetotransport properties of $Bi_{100-x}Sb_x$ topological insulator thin films prepared by flash evaporation *J. Phys. Chem. Solids* **167** 110734

[23] Compans E 1989 Dynamic method for *in situ* measurement of the thermoelectric power of vapor quenched thin films *Rev. Sci. Instrum.* **60** 2715

[24] Barzola-Quiquia J, Lauinger C, Zoraghi M, Stiller M, Sharma S and Häussler P 2017 Superconductivity in the amorphous phase of topological insulator Bi_xSb_{100-x} alloys *Supercond. Sci. Technol.* **30** 015013

[25] Buckel W and Hilsch R 1954 Einfluß der Kondensation bei tiefen Temperaturen auf den elektrischen Widerstand und die Supraleitung fuer verschiedene Metalle *Z. Phys.* **138** 109

[26] Buckel W 1959 Hall-Effekt von abschreckend kondensierten Wismutschichten *Z. Phys.* **154** 474

[27] Häussler P 1994 Interrelations between atomic and electronic structures—liquid and amorphous metals as model systems *Top. Appl. Phys.* **72** 163

[28] Barzola-Quiquia J, Osmic E, Bercoff P G, Venosta L and Häussler P 2023 Superconductivity in the amorphous phase of the half-Heusler TiNiSn alloy *J. Non-Cryst. Solids* **600** 121969

[29] Wu C Y, Jian W B and Lin J J 1995 Phonon-induced electron-electron interaction in disordered superconductors *Phys. Rev.* B **52** 15479

[30] Altshuler B L and Aronov A G 1985 Chapter 1—Electron–electron interaction in disordered conductors *Electron–Electron Interactions in Disordered Systems* (*Modern Problems in Condensed Matter Sciences* vol 10) ed A L Efros and M Pollak (Elsevier) pp 1–153

[31] Jian W B, Wu C Y, Chuang Y L and Lin J J 1996 lectron-electron interaction and normal-state transport in superconducting Ti-(Sn,Ge) alloys *Phys. Rev.* B **54** 4289

[32] Wu Y, Jian W B and Lin J J 1998 Electron-phonon scattering times in crystalline disordered titanium alloys between 3 and 15 K *Phys. Rev.* B **57** 11232

[33] Lin J J, Jian W B and Wu C Y 1998 Effective electron-electron interaction in superconducting Ti-(Sn,Ge) alloys *Czech. J. Phys.* **46** 759

[34] Hor Y S, Checkelsky J G, Qu D, Ong N P and Cava R J 2011 Superconductivity and non-metallicity induced by doping the topological insulators Bi_2Se_3 and Bi_2Te_3 *J. Phys. Chem. Solids* **72** 572

[35] Zhang J *et al* 2011 Band structure engineering in $(Bi1-xSb_x)_2Te_3$ ternary topological insulators *Nat. Commun.* **2** 574

[36] Zhang J *et al* 2015 Disentangling the magnetoelectric and thermoelectric transport in topological insulator thin films *Phys. Rev.* B **91** 075431

[37] Cao H, Venkatasubramanian R, Liu C, Pierce J, Yang H, Hasan M Z, Wu Y and Chen Y P 2012 Band structure engineering in $(Bi1-xSb_x)_2Te_3$ ternary topological insulators *Appl. Phys. Lett.* **101** 162104

[38] Pilidi A, Speliotis T and Litsardakis G 2020 Structural and magnetotransport characterization of magnetron sputtered co-doped Bi_2Te_3 thin films *J. Magn. Magn. Mater.* **511** 166971

[39] Qu D-X, Hor Y S, Xiong J, Cava R J and Ong N P 2010 Quantum oscillations and hall anomaly of surface states in the topological insulator Bi_2Te_3 *Science* **329** 821

[40] Bera S, Behera P, Venkatesh R and Ganesan V 2021 Magnetotransport and thermal properties of microwave synthesized nanostructured Bi_2Te_3 *J. Appl. Phys.* **129** 194304

[41] Lakhani A and Kumar D 2021 Observation of multichannel quantum coherent transport and electron-electron interaction in Bi_2Te_3 single crystal *Appl. Phys. Lett.* **114** 182101

[42] Wang J, DaSilva A, Chang C-Z, He K, Jain J, Samarth N, Ma X-C, Xue Q-K and Chan M 2011 Evidence for electron-electron interaction in topological insulator thin films *Phys. Rev.* B **83** 245438

[43] Lu H-Z and Shen S-Q 2014 Finite-temperature conductivity and magnetoconductivity of topological insulators *Phys. Rev. Lett.* **112** 146601

[44] Wang Q, Yu P, Huang X, Fan J, Jing X, Ji Z, Liu Z, Liu G, Yang C and Lu L 2018 Observation of weak anti-localization and electron-electron interaction on few-layer 1T′-$MoTe_2$ thin films *Chin. Phys. Lett.* **35** 077303

[45] Breznay N P, Volker H, Palevski A, Mazzarello R, Kapitulnik A and Wuttig M 2012 Weak antilocalization and disorder-enhanced electron interactions in annealed films of the phase-change compound $GeSb_2Te_4$ *Phys. Rev.* B **86** 205302

[46] Takagaki Y, Jenichen B, Jahn U, Ramsteiner M and Friedland K-J 2012 Weak antilocalization and electron-electron interaction effects in Cu-doped Bi_2Se_3 films *Phys. Rev.* B **85** 115314

[47] Lin J J, Hsu S Y, Lue J C and Sheng P J 2001 Spin–orbit scattering effect on electron–electron interactions in disordered metals *J. Phys. Chem. Solids* **62** 1813

[48] Roy A, Guchhait S, Sonde S, Dey R, Pramanik T, Rai A, Movva H C P, Colombo L and Banerjee S K 2013 Two-dimensional weak anti-localization in Bi_2Te_3 thin film grown on Si(111)-(7 × 37) surface by molecular beam epitaxy *Appl. Phys. Lett.* **102** 163118
[49] Liu H-C, Lu H-Z, He H-T, Li B, Liu S-G, He Q L, Wang G, Sou I K, Shen S-Q and Wang J 2014 Tunable interaction-induced localization of surface electrons in antidot nanostructured Bi_2Te_3 thin films *ACS Nano* **8** 9616
[50] He H-T, Wang G, Zhang T, Sou I-K, Wong G K L and Wang J-N 2011 Impurity effect on weak antilocalization in the topological insulator Bi_2Te_3 *J. Phys. Chem. Solids* **106** 166805
[51] Mallick D, Mandal S, Bitla Y, Ganesan R and Kumar P S A 2019 Emergence of electron-phonon coupling in a dual topological insulator BiTe *Mater. Res. Express* **6** 126321
[52] Kondo J 1964 Resistance minimum in dilute magnetic alloys *Prog. Theor. Phys.* **32** 37
[53] de Haas W J, de Boer J and van den Berg G J 1934 The electrical resistance of gold, copper and lead at low temperatures *Physica* **1** 1115
[54] Barzola-Quiquia J and Häussler P 2007 Electronic transport properties of amorphous and quasicrystals TM_xAl_{100-x} alloys *J. Non-Cryst. Solids* **353** 3237
[55] Hikami S, Larkin A I and Nagaoka Y 1980 Spin-orbit interaction and magnetoresistance in the two dimensional random system *Prog. Theor. Phys.* **63** 707
[56] Wang W J, Gao K H and Li Z Q 2016 Thickness dependent transport channels in topological inslator Bi_2Se_3 thin films grown by magnetron sputtering *Sci. Rep.* **6** 25291
[57] Kopp J 1975 Single impurity Kondo effect in gold: 1. Thermopower *J. Phys. F : Metal Phys.* **5** 1211
[58] Samanta M, Pal K, Waghmare U V and Biswas K 2020 Intrinsically low thermal conductivity and high carrier mobility in dual topological quantum material, n-type BiTe *Angew. Chem.* **132** 4852
[59] Wang X, He H, Wang N and Miao L 2013 Effects of annealing temperature on thermoelectric properties of Bi_2Te_3 films prepared by co-sputtering *Appl. Surf. Sci.* **276** 539
[60] Zhang G H, Qin H J, Teng J, Guo J, Guo Q L, Dai X, Fang Z and Wu K H 2009 Quintuple-layer epitaxy of thin films of topological insulator Bi_2Se_3 *Appl. Phys. Lett.* **95** 053114
[61] Shahil K M F, Hossain M Z, Goyal V and Balandin A A 2012 Crystal symmetry breaking in few-quintuple Bi_2Te_3 films: applications in nanometrology of topological insulators *J. Appl. Phys.* **111** 054305
[62] Secor J, Harris M A, Zhao L, Deng H, Raoux S and Krusin-Elbaum L 2014 Amorphous topological insulators constructed from random point sets *Appl. Phys. Lett.* **104** 221908
[63] Xu H, Song Y, Gong Q, Pan W, Wu X and Wang S 2015 Raman spectroscopy of epitaxial topological insulator Bi_2Te_3 thin films on GaN substrates *Mod. Phys. Lett.* B **29** 1550075
[64] Caha O *et al* 2013 Growth, structure and electronic properties of epitaxial bismuth telluride topological insulator films on BaF_2(111) substrates *Cryst. Growth Des.* **13** 3365
[65] Wang C, Zhu X, Nilsson L, Wen J, Wang G, Shan X, Zhang Q, Zhang S, Jia J and Xue Q 2013 *In situ* Raman spectroscopy of topological insulator Bi_2Te_3 films with varying thickness *Nano Res.* **6** 688
[66] Shahil K M F, Hossain M Z, Teweldebrhan D and Balandin A A 2010 Crystal symmetry breaking in few-quintuple Bi_2Te_3 films: applications in nanometrology of topological insulators *Appl. Phys. Lett.* **96** 153103
[67] Kullmann W, Geurts J, Richter W, Lehner N, Rauh H, Steigenberger U, Eichhorn G and Geick R 1984 Effect of hydrostatic and uniaxial pressure on structural properties and Raman active lattice vibrations in Bi_2Te_3 *Phys. Status Solidi* b **125** 131
[68] Bando H, Koizumi K, Oikawa Y, Daikohara K, Kulbachinskii V A and Ozaki H 2000 The time-dependent process of oxidation of the surface of Bi_2Te_3 studied by x-ray photoelectron spectroscopy *J. Phys.: Condens. Matter* **12** 5607
[69] Ahmad M, Agarwal K and Mehta B R 2020 An anomalously high seebeck coefficient and power factor in ultrathin Bi_2Te_3 film: spin–orbit interaction *J. Appl. Phys.* **128** 035108